

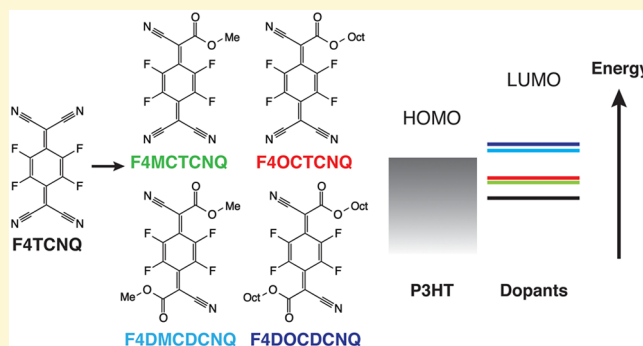
1 Introducing Solubility Control for Improved Organic P-Type Dopants

2 Jun Li,^{†,‡} Guangwu Zhang,^{†,§} Daniella E. Holm,[‡] Ian E. Jacobs,[‡] Bin Yin,[§] Pieter Stroeve,[‡] Mark Mascala,^{*,§}
3 and Adam J. Moule^{*,‡}

4 [†]Department of Chemical Engineering and Materials Science and [§]Department of Chemistry, University of California, Davis, United
5 States

6 **S** Supporting Information

7 **ABSTRACT:** To overcome the poor solubility of the widely
8 used p-type dopant 2,3,5,6-tetrafluoro-7,7,8,8-tetracyanoqui-
9 nodimethane (F4TCNQ), we have synthesized a series of
10 structure-modified, organic p-type dopants to include alkyl
11 ester groups designed to enable solubility and miscibility
12 control. UV–vis–NIR and cyclic voltammetry measurements
13 show increased solubility of mono- and diester substituted
14 dopants with only modest changes to acceptor strength. Using
15 UV–vis–NIR, photoluminescence, and in-plane conductivity
16 measurements, we demonstrate that the new dopants can
17 successfully p-type dope poly(3-hexylthiophene-2,5-diyl)
18 (P3HT). Monoester substituted dopants are characterized by
19 only slightly reduced electron affinity relative to F4TCNQ, but
20 greater doping effectiveness due to increased miscibility with P3HT. Diester substituted dopants undergo a dimerization reaction
21 before assuming their doped states, which may help anchor dopants into position post deposition, thus decreasing the negative
22 effect of dopant drift and diffusion. We conclude that increased dopant solubility/miscibility increases the overall effectiveness of
23 doping in solution-cast polymer films and that ester modification is a practical approach to achieving solubility/miscibility control
24 in TCNQ-type dopants.



25 ■ INTRODUCTION

26 Organic semiconductors have recently drawn much interest
27 because of a number of advantages they have over conventional
28 inorganic materials, which may include low cost, light weight,
29 compatibility with flexible substrates, biocompatibility, low
30 environmental impact, and chemical tailorability.^{1–4} Organic
31 electronic devices, such as organic light-emitting diodes
32 (OLEDs),^{5,6} organic photovoltaics (OPV),^{7,8} and organic
33 field-effect transistors (OFETs),^{9,10} show significant improve-
34 ments in performance with the addition of dopants. Intrinsic
35 organic semiconductors in general have low free-charge
36 densities and therefore low conductivity compared to inorganic
37 semiconductors. To increase conductivity, conjugated polymers
38 or small molecule semiconductors can be doped via the
39 addition (n-type) or removal (p-type) of electrons. One
40 method of doping a polymer is to form an organic salt using
41 acidic or basic doping groups for p- and n-type doping,
42 respectively.¹¹ Polyethylenedioxythiophene polystyrenesulfonate
43 (PEDOT:PSS) is a well-known example of an acidically
44 doped p-type organic conductive material.^{12,13} An alternative
45 method to dope organic semiconductors is to add a neutral
46 molecule with an electron affinity (EA) higher than the
47 ionization energy (IE) of the organic semiconductor.¹⁴ In this
48 case, an electron from the semiconductor is spontaneously
49 donated to the high EA molecule to create a hole state, a classic
50 example being the use of iodine to dope polythiophenes.^{15,16}

High EA organic molecular dopants have been studied since 51
the 1960s. Recent studies on such dopants have focused on the 52
role that ground state and excited state charge transfer (CT) 53
states play in quenching excited state fluorescence and in 54
recombination processes in OPV devices.^{17–20} Assuming no 55
CT-state formation, charge transfer occurs when the lowest 56
unoccupied molecular orbital (LUMO) of the dopant is 57
accessible to the highest occupied molecular orbital 58
(HOMO) of the organic semiconductor matrix. The dopant 59
molecule must also have a stable structure that can be 60
reoxidized without reaction with nearby molecules. The 61
quinone structure has these characteristics and early studies 62
of molecular organic dopants focused on tetrachlorobenzoqui- 63
none (chloranil; LUMO: –2.76 eV)^{21–23} and tetracyanoqui- 64
nodimethane (TCNQ; LUMO: –2.8 eV).^{24,25} More recently, 65
dopants with higher EA were prepared by incorporating 66
electron-withdrawing groups into the quinone ring. Dopants 67
in this category include 2,3-dichloro-5,6-dicyano-1,4-benzoqui- 68
none (DDQ; LUMO: –4.6 eV)^{26–28} and the more widely used 69
2,3,5,6-tetrafluoro-7,7,8,8-tetracyanoquinodimethane 70
(F4TCNQ; LUMO: –5.24 eV).^{14,29,30} Following the same 71
concept of molecular design, even higher EA dopants, such as 72
1,3,4,5,7,8-hexafluorotetracyanonaphthoquinodimethane (F6- 73

Received: June 18, 2015

Revised: July 20, 2015

74 TNAP; LUMO: -5.37 eV^{31,32} and 3,6-difluoro-2,5,7,7,8,8-
 75 hexacyanoquinodimethane (F2-HCNQ; LUMO: -5.59 eV),³³
 76 have been recently synthesized. Other recently reported p-type
 77 dopants with high EA include C₆₀ fullerene (LUMO: -3.6
 78 eV),³⁴ its fluorinated derivative C₆₀F₃₆ (LUMO: -5.38 eV),^{35,36}
 79 and hexaazatriphenylene hexacarbonitrile (HAT-CN6; LUMO:
 80 5.7 eV).^{37–39} However, most of these dopants have low
 81 solubility in common solvents, and are incorporated into
 82 devices structures using either evaporation processes^{14,40} or
 83 premixing in an inert matrix⁴¹ because they cannot be
 84 effectively solution processed. This limitation significantly
 85 restricts further development of solution-processed and mass-
 86 produced organoelectronics applications.⁴²
 87 In this paper, we first demonstrate a straightforward synthetic
 88 route to soluble versions of F4TCNQ-type dopants by
 89 substituting the cyano groups with either methyl or n-octyl
 90 esters (Figure 1). A comprehensive study of the electro-

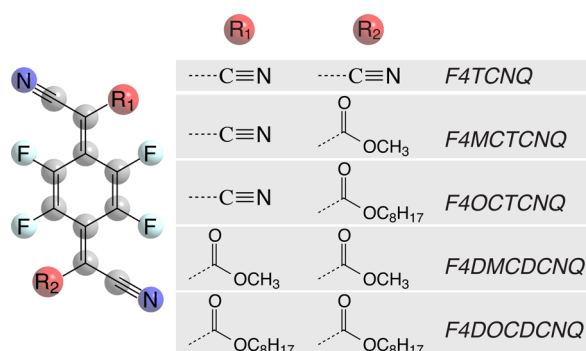


Figure 1. Molecular structures of F4TCNQ and its ester analogues.

91 chemical properties of these F4TCNQ analogues is performed
 92 using cyclic voltammetry. With a combination of optical
 93 absorption spectroscopy, photoluminescence spectroscopy, and
 94 conductivity measurements, we not only demonstrate the p-
 95 type doping of P3HT using these new dopants, but also show
 96 that comparable doping efficiency can be achieved even with
 97 slightly reduced electron affinity. These novel molecular
 98 dopants establish that the introduction of solubility control is
 99 a successful strategy to tailor the properties of organic p-type
 100 dopants.

101 ■ EXPERIMENTAL SECTION

102 **Materials.** 1,4-Bis(chloromethyl)-2,3,5,6-tetrafluorobenzene was
 103 purchased from Oakwood Products. Sodium hydride (60% dispersion
 104 in mineral oil) was purchased from Alfa Aesar. Bromine,
 105 perfluorobenzene, potassium carbonate, dimethyl carbonate, malono-
 106 nitrile, sodium acetate, sodium hydroxide, and phosphorus tribromide
 107 were purchased from Sigma-Aldrich. Anhydrous dimethyl sulfoxide
 108 (DMSO) and dimethylformamide (DMF) were purchased from Acros
 109 Organics. Hydrochloric acid (37% aqueous), p-toluenesulfonic acid
 110 monohydrate, ethanol, tetrahydrofuran (THF), dichloromethane
 111 (DCM), ethyl acetate, toluene, and hexane were purchased from
 112 Fisher Scientific. Acetic acid and sodium cyanide were purchased from
 113 Fluka. Octanol was purchased from EM Science. Trifluoroacetic acid
 114 (TFA) and acetic anhydride were purchased from EMD. P3HT
 115 (Regioregular >98%, $M_n = 54\text{--}75$ kDa, HOMO 5 eV and LUMO 3
 116 eV) was purchased from Sigma-Aldrich. F4TCNQ (>98%) was
 117 purchased from TCI. All chemicals were used as received unless
 118 otherwise indicated. All solvents were dried over molecular sieves (3
 119 Å) before use.

120 **Characterization.** ¹H NMR (300 MHz), ¹³C NMR (75 MHz) and
 121 ¹⁹F-NMR (282 MHz) spectra were recorded on a Varian Mercury 300

NMR spectrometer. Spectral data were processed using MestReNova 122
 (version 6.2.0) desktop NMR data processing software. 123

Cyclic voltammograms (CVs) were recorded on a BASi Epsilon 124
 MF-9092 Electrochemical Workstation. The redox potentials of all of 125
 substrates were measured in anhydrous acetonitrile (MeCN) solution 126
 containing tetramethylammonium tetrafluoroborate (Me₄NBF₄, 127
 0.05M) using a platinum disk ($\Phi = 1.6$ mm) as the working electrode 128
 and Ag/AgCl as the reference electrode. The concentration of 129
 substrates in the working solution was 0.5 mM, and the electro- 130
 chemical potential sweep rate was fixed at 100 mV/s. 131

High resolution mass spectra (HRMS) were obtained on a Thermo 132
 Fisher Hybrid LTQ-Orbitrap XL mass spectrometer equipped with 133
 electrospray. Liquid chromatography–mass spectra (LC-MS) were 134
 recorded on Qtrap LC/MS instruments. 135

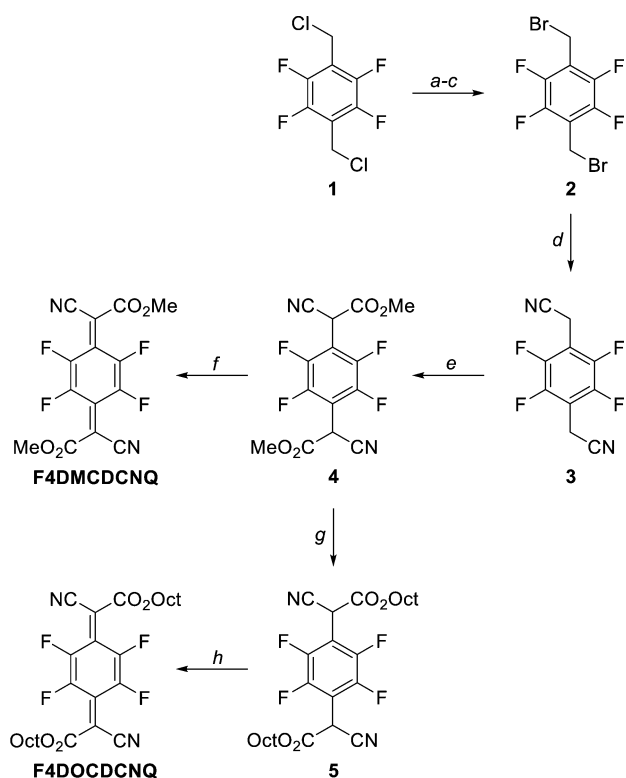
UV–vis–NIR and photoluminescence spectra were recorded on a 136
 PerkinElmer Lambda 750 spectrophotometer and a Varian Eclipse 137
 photoluminescence spectrophotometer, respectively. For the solubility 138
 measurements, 5 mg of F4TCNQ and 100 mg of the four new dopants 139
 were introduced into 1.0 mL of chloroform. The mixtures were stirred 140
 on a hot plate at 60 °C for 24 h, and then rested at room temperature 141
 for another 24 h. Saturated solutions were diluted accordingly in order 142
 to be measured in a useful absorbance range. Calibration curves were 143
 also measured for each dopant. For characterization of the blended 144
 films, glass substrates were cleaned in ultrasonic baths of acetone, 145
 Mucosal detergent (5%), and deionized water, followed by drying with 146
 nitrogen. The substrates were then exposed to UV/ozone for 30 min 147
 before use. Solutions of 5 mg/mL P3HT and p-type dopants (0.5 mg/ 148
 mL for F4TCNQ and 5 mg/mL for the ester derivatives) in 149
 chloroform were mixed in appropriate ratios to achieve the desired 150
 mole fraction of dopants to P3HT. Except neat F4TCNQ, all other 151
 films were spin-coated from blend solutions at 60 °C inside a nitrogen 152
 glovebox. Neat F4TCNQ films were deposited using an MBruan 153
 thermal evaporator at deposit rate ~ 0.2 Å/s. Film thicknesses were 154
 measured with a Veeco Dektak 150 Surface profilometer. All UV–vis– 155
 NIR and photoluminescence spectra were measured under ambient 156
 conditions in air. 157

Conductivity measurements were performed with a four-point 158
 probe setup using a Keithely 2420 source sourcemeter unit. Four 159
 electrodes (5 nm Cr/95 nm Au, 1×5 mm², 1 mm spacing) were 160
 deposited through a shadow mask by thermal evaporation. The same 161
 procedure was used for substrate cleaning and blended film deposition 162
 described above. All conductivity measurements were performed in the 163
 dark under a nitrogen atmosphere in a glovebox. 164

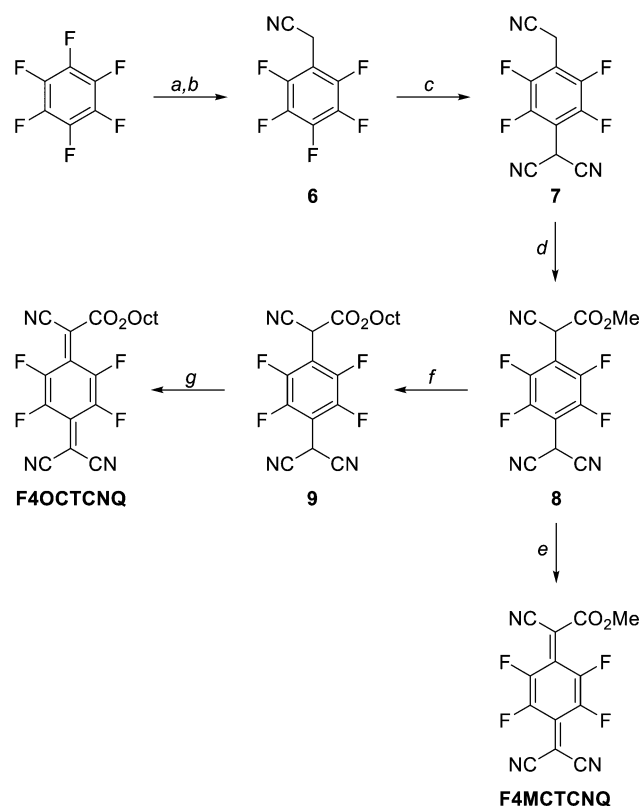
165 ■ RESULTS AND DISCUSSION

Synthesis of P-Type Dopants. Synthesis of the sym- 166
 metrical di(alkoxycarbonyl)dicyanotetrafluoroquinodimethanes 167
 F4DMCDCNQ and F4DOCDNQ starts from commercial 168
 1,4-bis(chloromethyl)-2,3,5,6-tetrafluorobenzene **1** (Scheme 1) 169 s1
 170 s1
 171 does not take place by direct substitution with cyanide, so the 172
 intermediate bis(bromomethyl)tetra-fluorobenzene **2** was 173
 prepared. Remarkably, direct substitution of **1** with bromide 174
 also proves challenging, but **2** could be made via the 175
 corresponding (bis)benzyl alcohol. Substitution of **2** with 176
 cyanide is facile, and methoxycarbonylation of **3** by 177
 deprotonation and reaction with dimethyl carbonate gives 178
 diester **4**. Oxidation of **4** to the dimethyl ester F4TCNQ 179
 analogue F4DMCDCNQ with bromine proceeds in high yield. 180
 Alternatively, transesterification of **4** with octanol gave the 181
 longer-chain diester **5**, which could likewise be readily oxidized 182
 to F4DOCDNQ. 183

The synthesis of the mono(alkoxycarbonyl)- 183
 tetrafluorotriacyanoquinodimethanes F4MCTCNQ and 184
 F4OCTCNQ starts from commercial hexafluorobenzene 185
 (Scheme 2). Reaction with methyl cyanoacetate in the presence 186 s2
 of a base gives the intermediate methyl 2-cyano-2- 187

Scheme 1. Synthesis of F4DMCDCNQ and F4DOCDNQ^a

^aReagents and conditions: (a) NaOAc, Ac₂O, AcOH, 105 °C, 36 h; (b) NaOH, EtOH/THF/H₂O, 75 °C, 24 h; (c) PBr₃, DCM, 10 h, 76% over 3 steps; (d) NaCN, CF₃COOH, DMSO, 5 h, 51%; (e) (MeO)₂CO, NaH, THF, 75 °C, 18 h, 83%; (f) Br₂, H₂O, 2 h, 94%; (g) octanol, TsOH·H₂O, toluene, 110 °C, 6 h, 72%; (h) Br₂, H₂O, 3 h, 93%.

Scheme 2. Synthesis of F4MCTCNQ and F4OCTCNQ^a

^aReagents and conditions: (a) MeOCOCH₂CN, K₂CO₃, DMF, 115 °C, 6 h, 72%; (b) 50% aq HOAc, conc. H₂SO₄, reflux, 15 h, 75%; (c) CH₂(CN)₂, NaH, THF, 70 °C, 18 h, 66%; (d) (MeO)₂CO, NaH, THF, 80 °C, 48 h, 89%; (e) Br₂, H₂O, 1 h, 82%; (f) octanol, TsOH·H₂O, toluene, 85 °C, 9 h, 71%; (g) Br₂, H₂O, 1.5 h, 81%.

188 (pentafluorophenyl)acetate, which is decarboxylated in situ to
189 give 2-(pentafluorophenyl)ethanenitrile **6**. S_NAr substitution
190 with the sodium salt of malononitrile provides **7**, which is
191 methoxycarbonylated by reaction with dimethyl carbonate and
192 base to give **8**. Oxidation of **8** with bromine gives
193 **F4MCTCNQ**, the monomethyl ester analogue of F4TCNQ.
194 Transesterification of **8** with octanol followed again by
195 oxidation gives the mono-octyl ester dopant **F4OCTCNQ**.
196 Detailed synthetic procedures are provided in the [Supporting](#)
197 [Information](#).

198 **Characterization of P-Type Dopants.** Our dopant design
199 goal was to improve the solubility of the dopant molecules
200 without compromising doping efficiency. To demonstrate the
201 improved solubility of the new F4TCNQ analogues, saturated
202 solutions were prepared in chloroform ([Figure 2a](#)) and their
203 absorbance spectra were recorded by UV–vis–NIR at room
204 temperature. The solubility limits ([Figure 2b](#)) were then
205 determined based on calibration curves of each compound. The
206 details of the calibration curves and measurements can be found
207 in the [Figure S47](#). As can be seen from [Figure 2b](#), the solubility
208 of the ester-substituted dopants is significantly greater than
209 F4TCNQ itself, by a factor of at least 55 for F4MCTCNQ and
210 100 for F4OCTCNQ. Interestingly, although the solubility of
211 the diesters are still ~30 times higher than that of F4TCNQ,
212 they are less soluble than the monoesters, which is attributed to
213 the higher symmetry of the diesters.⁴³

214 Because the EA of the dopant is an important predictor of
215 doping efficiency, the next thing we needed to show is what

effect substitution of an ester group for a cyano group on the
F4TCNQ structure would have on the reduction potential. The
electrochemical states of the dopants were investigated using
cyclic voltammetry (CV). Solutions of dopants in acetonitrile
were measured under reducing potentials and the CV data are
shown in [Figure 3a](#). As expected, F4TCNQ itself undergoes
two reversible one-electron reduction steps corresponding to
F4TCNQ^{•-} and F4TCNQ²⁻. The monoester-substituted
dopants F4MCTCNQ and F4OCTCNQ also exhibit two
reduction peaks, but interestingly, they are located between the
first and second reductions of F4TCNQ, and the first reduction
peak E_{red1} of the monoester-substituted dopants is greater than
the second reduction peak E_{red2} . Unlike F4TCNQ, only one
reduction peak is seen in the CV of diester-substituted dopants.
Closer inspection of the CV data reveals that both the mono
and diesters undergo redox processes that are either irreversible
or quasi-reversible. Therefore, instead of using the mean values
of anodic and corresponding cathodic peak potentials ($E_{1/2}$),
reduction potentials were used for comparison. The reduction
potentials for all dopants vs Ag/AgCl are summarized in [Table](#)
1.

As can be seen from [Table 1](#), E_{red1} shows a decreasing trend
from 0.51 to ~0.4 and ~0.2 V as cyano groups are substituted
by one or two ester groups, respectively, showing that
F4TCNQ is a stronger p-type dopant than its ester analogues.
This is expected since the cyano group is more electron
withdrawing than the ester group, which results in a more
electron deficient quinoid ring in the F4TCNQ than in the

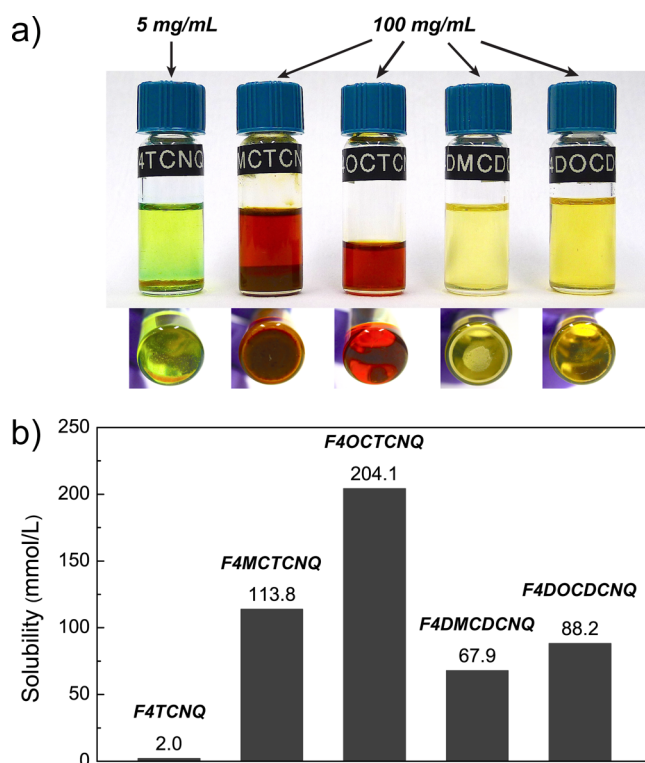


Figure 2. (a) Photos of saturated solutions (from left to right: F4TCNQ, F4MCTCNQ, F4OCTCNQ, F4DMCDCNQ, and F4DOCDCNQ) in chloroform. (b) Measured solubility limits of the dopants in chloroform at room temperature.

Table 1. Summary of Reduction Potentials from CV and Determined LUMO Levels of F4TCNQ and Its Ester Derivatives

compd	E_{red1} (V)	E_{LUMO1} (eV)	E_{red2} (V)	E_{LUMO2} (eV)
F4TCNQ	0.51	-5.23	0	-4.72
F4MCTCNQ	0.42	-5.14	0.12	-4.84
F4OCTCNQ	0.40	-5.12	0.11	-4.83
F4DMCDCNQ	0.25	-4.97		
F4DOCDCNQ	0.21	-4.93		

ester-substituted derivatives. Comparing the octyl and methyl ester substituted dopants, subtle differences in E_{red1} are observed. Longer alkyl chains are more electron donating so the E_{red1} values of the methyl ester-substituted dopants are slightly greater than those of the octyl ester derivatives, increasing from 0.40 to 0.42 V and from 0.21 to 0.25 V, for the monoester and diester derivatives, respectively.

On the basis of the CV data, the LUMO levels for each dopant can be determined from their reduction potentials according to following relationship: $E_{\text{LUMO}} = -e(E_{\text{red}} + E_{\text{ref}})$, where E_{ref} is 4.72 V for the Ag/AgCl reference electrode used in our measurements.^{33,44,45} The measured LUMO energies are also listed in Table 1. The measured LUMO level of F4TCNQ (-5.23 eV) is in good agreement with the published values from CV (5.33 eV)³³ as well as ultraviolet photoelectron spectroscopy (UPS) (5.24 eV),⁴⁶ which verifies the accuracy of our assignments.

To enable a visual comparison, the LUMO levels of all investigated p-type dopant molecules are compiled into one energy diagram (Figure 3b). The HOMO and LUMO levels of P3HT and P3HT positive polaron (P3HT⁺) reported from literature^{15,47-49} are also shown to scale. Further discussion of

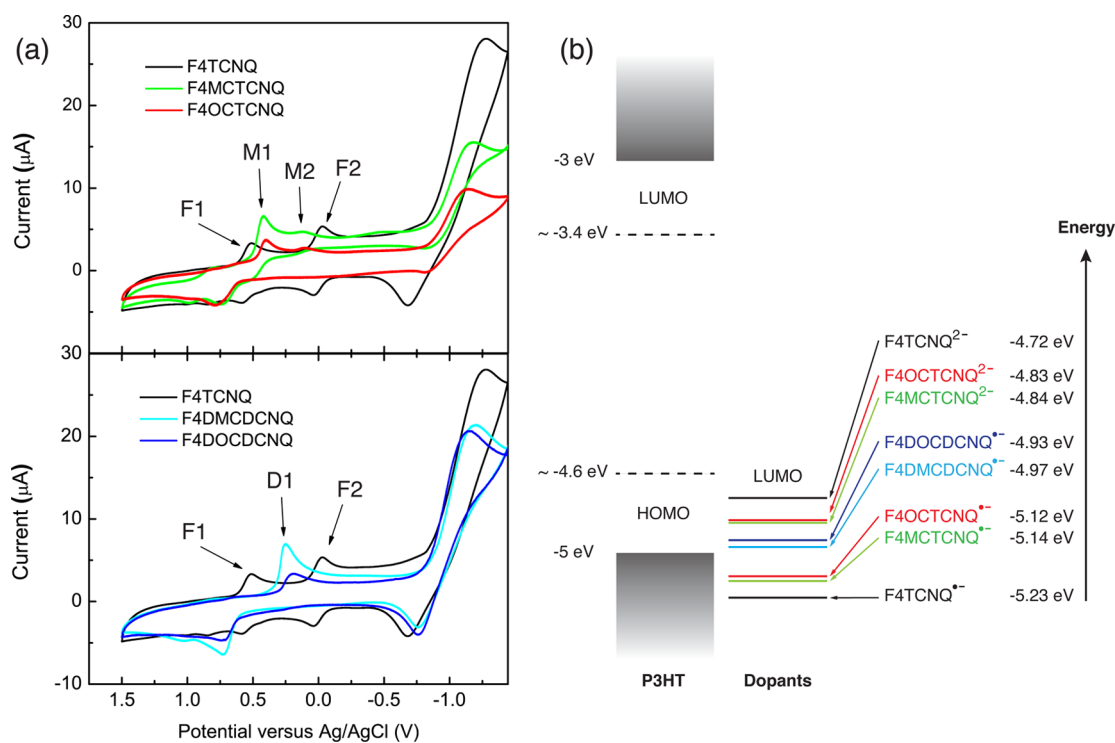


Figure 3. (a) Cyclic voltammograms of F4TCNQ and its monoester derivatives (top) and diester derivatives (bottom). Reduction potentials of F4TCNQ (F1, F2), monoester derivatives (M1, M2), and diester derivatives (D1) are marked. (b) Molecular orbital energy level diagram of P3HT (left: solid line for neutral P3HT and dashed line for P3HT polaron) and p-type dopants (right).

266 the P3HT matrix/dopants system is deferred to the next
 267 section, as we focus here on the comparison of LUMO levels of
 268 the dopants. Similar to F4TCNQ, E_{red1} and E_{red2} for the ester
 269 analogues can be assigned to the formation of anion radicals
 270 from the neutral molecules and the formation of dianions from
 271 the anion radicals, respectively. Therefore, we assign singly and
 272 doubly reduced dopants as compound $^{\bullet-}$ and compound $^{2-}$,
 273 respectively. Among the compounds considered, F4TCNQ
 274 shows the deepest LUMO level, F4MCTCNQ $^{\bullet-}$ and
 275 F4OCTCNQ $^{\bullet-}$ show the next deepest levels, and
 276 F4DMCDCNQ $^{\bullet-}$ and F4DOCDNQ $^{\bullet-}$ show relatively
 277 shallow levels. In addition, doubly reduced dopants show
 278 weaker reduction strength (smaller EA) and thereby shallower
 279 LUMO levels than singly reduced dopants, as expected.
 280 Another highlight of the CV measurements is that there is
 281 only one reduction peak for diester-substituted dopants. Thus,
 282 the LUMO levels of F4DMCDCNQ $^{2-}$ and F4DOCDNQ $^{2-}$
 283 are not shown because these species do not form based on the
 284 CV data. This suggests that the diester-substituted dopants
 285 undergo a different chemical process during reduction than the
 286 F4TCNQ and monoester-substituted dopants, the details of
 287 which will be discussed below. Finally, only subtle differences in
 288 LUMO levels are found between the methyl ester and octyl
 289 ester analogues, merely 0.01–0.04 eV, indicating that the R
 290 group on the ester does not strongly influence the electronic
 291 nature of the TCNQ dopants.

292 A mechanism is proposed to explain the charge transfer
 293 processes of F4TCNQ and ester-substituted dopants, as
 294 illustrated schematically in Figure 4. Assuming only one
 295 electron is involved at each step, radical anions are formed

from neutral molecules in the first reduction. Resonance
 structures are also shown. Due to the molecular symmetry of
 the F4TCNQ and the diester molecules, the two resonance
 structures of their anion radicals are identical, whereas for the
 monoester molecules, the spin and negative charge density may
 be asymmetrically distributed. By accepting a second electron,
 dianions are formed subsequently for F4TCNQ and the
 monoesters. However, this is not the case for the diester
 molecules. Instead, radical coupling takes place to give a
 dimeric dianion. Only one reduction potential is observed,
 suggesting that the radical coupling is rapid and irreversible.

To support the above hypothesis, we measured the masses of
 the fully reduced dopant molecules using mass spectrometry
 (MS). F4TCNQ and all four ester-substituted analogues were
 mixed with potassium iodide (KI) to ensure full reduction,
 and the resulting mass spectra are shown in the Figures S37–S46.
 From these data, it is clear that diester dopants form dimers
 after reduction while monoester dopants and F4TCNQ do
 not. The structure of the dimer shown in Figure 4 is a proposal
 based on the most likely site for spin coupling, involving no
 interference with the aromaticity of the benzene rings and with
 maximum possible separation of the charges. However, for the
 purposes of this work, the exact structure of the dimer is of no
 real consequence.

Characterization of Doped Films. It has been shown in
 the above sections that F4TCNQ can be synthetically altered to
 incorporate esters in place of nitrile groups, where the ester can
 support different alkyl chains that can be used to affect the
 solubility of the molecule. In this section we demonstrate
 successful p-type doping of the well-characterized conjugated
 polymer P3HT by the above-described ester-substituted
 dopants. In particular, we investigate the effect of altering the
 solubility of the dopant on the charge density and conductivity
 of the polymer.

Measuring Charge Density. Absorption spectroscopy (UV–
 vis–NIR) is commonly used to observe changes in the
 crystalline to amorphous content of P3HT samples.^{50,51} The
 doping level can also be monitored using UV–vis–NIR.³⁰
 Grazing incidence X-ray spectra and concentration-dependent
 conductivity were recently measured for the P3HT/F4TCNQ
 system.⁵² For doping levels below 4 mol %, F4TCNQ occupies
 locations within the amorphous part of the P3HT⁵² but dopes
 exclusively in the crystalline domains.²⁰ Between 4 mol % and
 17 mol % doping ratios, F4TCNQ intercalates between the
 P3HT chains within crystalline domains, increasing the (010)
 crystal spacing (along the π -stacking direction) from 3.83
 to 7.18 Å.⁵² The 17 mol % blend ratio is the point when this
 blend system reaches the upper limit on both conductivity and
 low energy absorptivity (1–1.7 eV) according to literature.⁵²

The normalized UV–vis–NIR absorption spectra for P3HT/
 dopant at selected doping ratios are shown in Figure 5. The full
 doping concentration series of UV–vis–NIR spectra can be
 found in the Supporting Information (Figure S48). These data
 exactly reproduce the literature results for P3HT/F4TCNQ.⁵²
 Undoped P3HT has a band gap of \sim 1.9 eV. Upon oxidation by
 F4TCNQ, two broad sub-bandgap absorbance peaks centered
 around 0.4 and 1.5 eV are observed, which can be assigned to
 the polarons of P3HT.^{53,54} In addition, two sharper peaks at
 1.43 and 1.62 eV can be detected that correspond to
 absorbance by F4TCNQ $^{\bullet-}$. As shown in Figure 5, subgap
 absorbances similar to those of F4TCNQ $^{\bullet-}$ are seen in
 F4MCTCNQ $^{\bullet-}$ and F4OCTCNQ $^{\bullet-}$. The double peaks at
 1.43 and 1.62 eV are replaced by a single absorbance at the

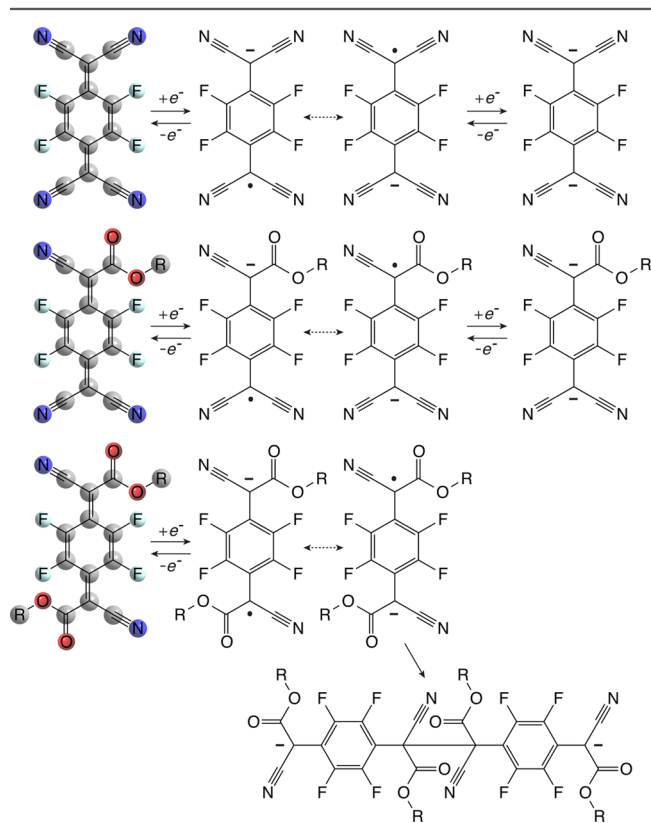


Figure 4. Proposed mechanism for charge transfer for F4TCNQ and its derivatives. The –R group can be a methyl or octyl group. Resonance structures for the radical anions are also displayed.

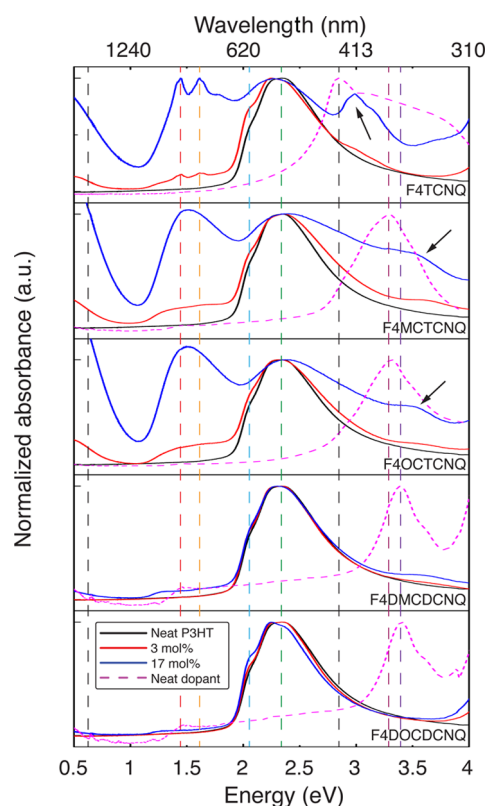


Figure 5. Normalized UV-vis-NIR absorbance spectra of neat P3HT (black), dopants (magenta dashed line), and P3HT/dopant blend films at 3 mol % (red) and 17 mol % (blue) doping ratios. Arrows show the dedope peak for P3HT/dopant system.

359 same energy that increases with increased dopant concen-
 360 tration. In fact, the NIR absorbance is stronger at both 0.4 and
 361 1.5 eV in films doped with the monoester dopants than with
 362 F4TCNQ at the same mol % doping concentration. For
 363 instance, at 17 mol % the ratios between polaron absorbance at
 364 1.5 eV to ground-state absorbance at 2.3 eV are 1:1, 1.04:1, and
 365 1.12:1 for F4TCNQ, F4MCTCNQ and F4OCTCNQ,
 366 respectively. The increased polaron/ground-state ratio is an
 367 indication that higher P3HT polaron density is achieved for
 368 monoester derivatives. Conversely, only a slight increase in
 369 P3HT polaron peaks is observed in films containing
 370 F4DMCDCNQ and F4DOCDCNQ, even as the doping
 371 concentration reaches 17 mol %. This result indicates that
 372 there is less charge transfer between P3HT and the diester
 373 dopants compared with the F4TCNQ and monoester dopants
 374 at the same doping concentration.

375 Changes in the short-range ordered regions (aggregates)^{55,56}
 376 of P3HT can be probed by monitoring the absorbance ratio of
 377 the 0–0 to 0–1 vibronic peaks at 2.03 eV (610 nm) and 2.25
 378 eV (550 nm) because these peak are associated with interchain-
 379 delocalized excitation^{47,57} and the degree of P3HT order-
 380 ing.^{55,58,59} The concentration-dependent spectra in the Figure
 381 S48 show that the relative intensity of the peak at 610 nm
 382 compared to the other P3HT vibronic peaks increases with
 383 increasing doping concentration up to 10 mol %. This result
 384 implies one of two things. It could indicate that crystalline
 385 domains of P3HT are becoming more ordered (more planar)
 386 upon doping. Alternatively, the relative increase in the peak at
 387 2.03 eV could indicate an increased probability of doping in less
 388 crystalline domains. The ground-state signal is bleached upon

doping and only the most crystalline sections of the sample are
 389 isolated from contact with the dopants. A relative increase in
 390 the peak at 610 nm occurs in all P3HT/acceptor systems,
 391 although the diester dopants induce less pronounced shifts in
 392 the vibronic spectra.
 393

Besides the characteristics of the doping effects mentioned
 394 above, UV-vis-NIR spectra for all neat dopants are also
 395 presented. The absorbance spectra of these five dopants do not
 396 show many differences other than the broader and red-shifted
 397 absorption peak for F4TCNQ. The blueshift of the absorption
 398 peak from F4TCNQ (~2.8 eV) to the monoester derivatives
 399 (~3.3 eV) and diester derivatives (~3.4 eV) is expected due to
 400 less delocalization of charge resulting from replacing cyano with
 401 ester groups. The appearance of an additional peak in the high
 402 energy range of blend systems is also noted, as indicated by
 403 arrows (Figure 5). These peaks are assigned to the dopant
 404 anion, although in monoester systems an overlapping of the
 405 monoester anion absorbance and neutral dopant molecule
 406 absorbance is observed. A recent study from our group showed
 407 that this optical transition can be used to dedope P3HT/
 408 F4TCNQ films with complete recovery of optical character-
 409 istics and mobilities.⁶⁰ The related transitions for ester-
 410 substituted dopants are blue-shifted with respect to F4TCNQ
 411 by ~0.5 eV. The UV-vis-NIR spectra of the dopant anions
 412 can be found in the Figure S49.
 413

The differential solubility of the mono- and diester dopants
 414 with methyl and octyl chains enables us to evaluate the effect of
 415 dopant solubility on doping efficiency, with the long chain
 416 esters showing higher solubility. Comparison of the P3HT⁺/
 417 dopant⁻ CT-state absorbance features to the ground-state
 418 absorbance of bulk P3HT gives a direct measure of the charge
 419 density. The results in this section clearly indicate that a dopant
 420 that is more miscible in the polymer has a higher probability of
 421 doping the polymer.
 422

Measuring Dopant Miscibility. Photoluminescence spec-
 423 troscopy (PL) is another technique that has been extensively
 424 used to evaluate doping interactions in organic materials
 425 because photoluminescence is quenched by the presence of
 426 dopants.^{53,61} Dopants increase the free charge density in the
 427 polymer and free charges react with and quench excitons
 428 through a dark process with $\sim 1/r^3$ distance dependence.⁶² PL
 429 experiments were performed using 2.4 eV excitation to optically
 430 excite P3HT and the PL emission for undoped P3HT (1.4–2.0
 431 eV) was observed. Figure 6 shows the PL intensity as a function
 432 of mol fraction for all dopants. The inset shows typical PL
 433 spectra for neat and doped P3HT at 1 mol % doping ratio. As
 434 can be seen, F4DMCDCNQ and F4DOCDCNQ show only
 435 partial PL quenching of ~20% and ~40%, respectively.
 436 F4TCNQ is a stronger exciton quencher (~80%), whereas
 437 monoester dopants F4MCTCNQ and F4OCTCNQ are able to
 438 fully quench PL. This result clearly indicates that 20% of the
 439 P3HT volume remains undoped by F4TCNQ at 1 mol %
 440 doping ratio, while all P3HT domains are infiltrated by
 441 monoester-substituted dopants at the same concentration. The
 442 full concentration series of PL spectra can be found in the
 443 Figure S48. Unlike the monoester dopants where complete
 444 quenching occurs at lower than 1 mol % doping, complete
 445 quenching for diester dopants is observed at around 17 mol %.
 446 This is consistent with dimerization of the dopants, which
 447 causes charging of P3HT at higher dopant concentrations.
 448

To summarize, on the basis of the reduction potential of the
 449 dopants, F4TCNQ should be a more effective dopant than the
 450 mono- and diester dopants by 0.2 and 0.4 eV, respectively.
 451

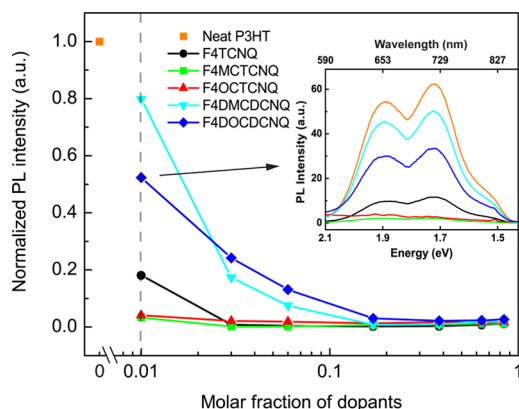


Figure 6. Normalized photoluminescence intensity as a function of doping concentration for all P3HT/dopant systems. Inset: PL quenching at 1 mol % doping ratio. The full doping concentration series of spectra can be found in the [Supporting Information](#).

452 However, UV-vis-NIR results indicate that monoester-
453 substituted TCNQs generate more charge density in P3HT
454 at the same doping ratio. PL quenching demonstrates that
455 monoester dopants infiltrate all domains of P3HT at a lower
456 concentration than F4TCNQ. These results are in consistent
457 with the increased solubility of dopants in CHCl_3 .

458 **Conductivity.** In this section, we describe concentration-
459 dependent conductivity measurements that were performed to
460 determine whether the increase in dopant miscibility translates
461 to enhanced electronic properties. [Figure 7a](#) shows a log-log
462 plot of conductivity versus mole fraction of dopant for P3HT
463 doped with F4TCNQ and each of the new dopants. Blend films

at different doping ratios were spin-cast on prepatterned 464
substrates and then measured by the four-point probe method, 465
the details of which have been described in earlier 466
publications.^{63,64} It is clear that the in-plane conductivity of 467
P3HT can be tuned by at least 3 orders of magnitude by all 468
dopants. All dopants also show a similar trend of increased 469
conductivity with increasing dopant concentration. After 470
reaching a peak, the addition of more dopant leads to an 471
increase in neutral dopant domains and conductivity decreases 472
with increased concentration. The upper limit of conductivity 473
in P3HT when doped with F4TCNQ or monoester dopants is 474
 $\sim 10^0$ S/cm while for diester dopants the maximum 475
conductivity is $\sim 1 \times 10^{-1}$ S/cm. 476

Over most of the doping range, the conductivity of P3HT 477
doped with the monoester dopants is higher at the same mole 478
fraction than P3HT doped with F4TCNQ, which is consistent 479
with UV-vis-NIR and PL measurement results. For 480
comparison to the earlier work of Duong et al.,⁵² the 481
conductivity data are also plotted on a log linear scale ([Figure](#) 482
[7b](#)). Just as was seen for P3HT doped with F4TCNQ, there is a 483
clear change in the slope of conductivity vs concentration for all 484
dopants at around 4 mol % dopant loading. We assume here 485
that the assignments made by Duong et al. are correct in that 486
the initial high slope comes from dopants mixing into the 487
amorphous P3HT domains.^{20,52} At higher doping ratios, the 488
dopants intercalate into the crystalline P3HT domains, 489
increasing the crystal spacing between P3HT chains. The 490
initial slopes for loading of dopant up to 4 mol % are identical 491
for the monoester dopants and F4TCNQ. However, when the 492
doping ratio is increased beyond 4 mol %, F4OCTCNQ in 493
particular shows a larger increase in conductivity with increased 494

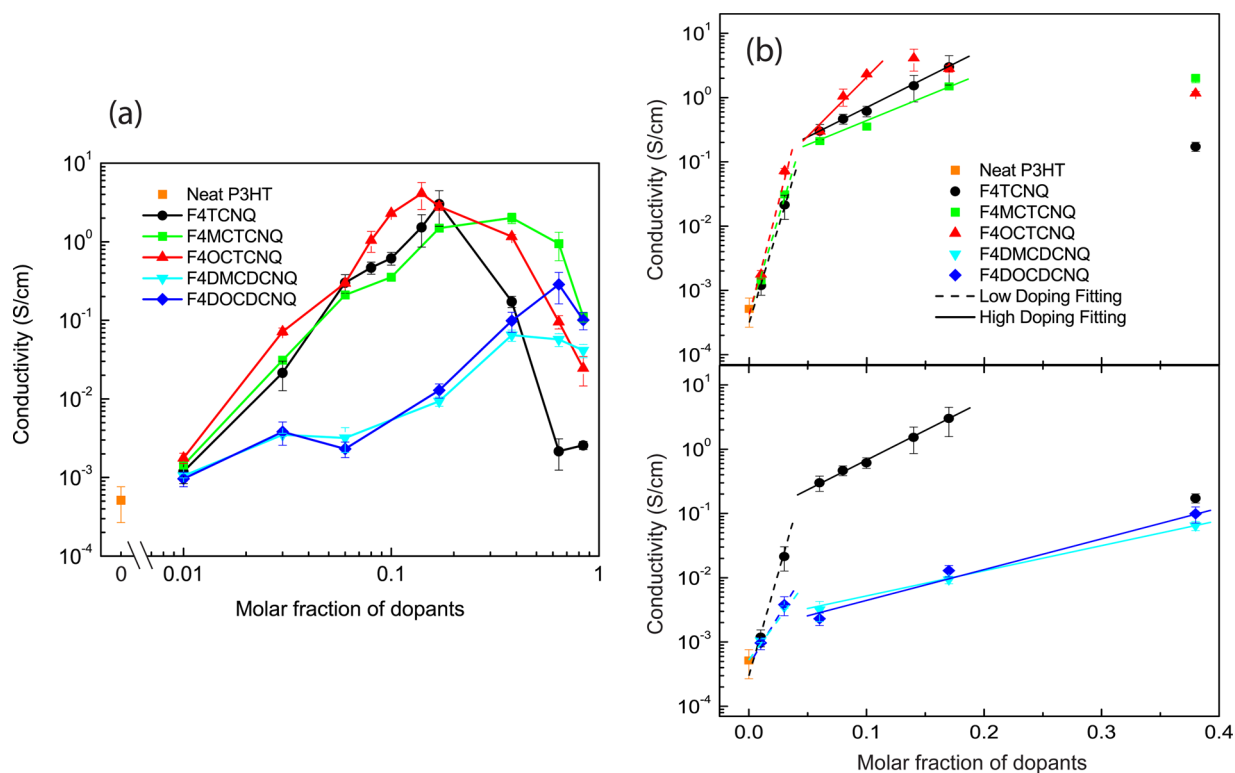


Figure 7. (a) In-plane conductivity measurements of P3HT/dopant blend films as a function of doping concentration. The neat P3HT film conductivity is also shown (orange). (b) Fits to the conductivity data in the weak (dashed lines) and strong (solid lines) doping regimes for F4TCNQ and the monoester derivatives (top) and diester derivatives (bottom).

doping than F4TCNQ, confirming that the modified dopant is more efficient at intercalating between P3HT chains. This result demonstrates that increased miscibility of the dopant has a clear advantage for doping efficiency. For F4TCNQ, the peak in conductivity occurs at 17 mol % doping followed by a rapid drop in conductivity with increased dopant concentration, presumably because increased dopant content is neutral and pure F4TCNQ crystals are formed in the polymer.⁵² By comparison, both monoester dopants show a much broader peak in conductivity with increased dopant concentration, which also argues for better miscibility between the dopant and P3HT.

Another interesting observation is that the conductivity of P3HT samples doped with diester dopants increases exponentially up to 40 mol % doping ratio, whereas the F4TCNQ and monoester dopants show an exponential increase in conductivity until 10 mol % for F4OCTCNQ and 17 mol % for F4MCTCNQ and F4TCNQ, respectively. This is consistent with the UV-vis-NIR results for the diesters (Figure S48) which show that P3HT polaron density continues to increase with up to 64 mol % dopant loading. This trend cannot be explained solely by the relatively shallow LUMO level of diesters. Instead, the increase in conductivity with such high doping levels implies that the dimerization reaction stabilizes the doped states. The conductivity does not increase until there is high enough dopant concentration that they are able to dimerize and form stable dianions. This dimerization reaction shifts equilibrium toward the dianion, which is trapped by the irreversibility of the process and then cannot give the electron back into the polymer. Although it may be considered disadvantageous that large doping ratios are necessary to achieve higher conductivity with the diesters, there is a possible processing advantage to the dimerization reaction. This advantage is that the large dianion is unlikely to diffuse with thermal stress or drift with electric field stress. The smaller F4TCNQ is known to diffuse against a concentration gradient and thereby to dope regions of the sample outside of the originally intended area, thus reducing device lifetimes.³⁵ In addition, because the diester-substituted dopants do not dimerize until after deposition, they can be efficiently mixed into the polymer and then doping can occur post film formation through the dimerization reaction. The dopants, once dimerized, will provide a much higher barrier to diffusion.

CONCLUSIONS

In conclusion, we have developed a method to introduce solubility control into p-type organic dopants based on the F4TCNQ structure. Solubility control is achieved by replacing cyano groups on the F4TCNQ framework with ester groups. The results show that the solubility of the new ester dopants is improved by a factor of at least 30 and up to 100 compared with F4TCNQ at room temperature. In addition, these new dopants possess a range of interesting properties. First, monosubstituted ester dopants show only slightly lower (~0.2 eV) electron affinity than F4TCNQ. However, in spite of the lower EA, monoester dopants lead to increased polaron density and more efficient doping in P3HT than F4TCNQ. F4OCTCNQ, for instance, has the same conductivity at 10 mol % doping as F4TCNQ at 17 mol % doping. The increased doping efficiency is proposed to be a result of the ester-substituted dopants being both more soluble in good solvents for P3HT and more miscible in P3HT itself. This study not only shows that molecular tailoring of organic dopants for

increased miscibility with the desired polymer is a sound approach to improving doping efficiency, but also that single ester replacements are a viable method to modify common dopant structures with cyano attachments. Additionally, we also introduce diester-substituted dopants, which have distinctly different electrochemical properties than F4TCNQ and the monoester dopants due to a dimerization reaction that occurs between their radical anions. Despite the shallow LUMO level of the diesters, this irreversible dimerization also results in effective doping. However, much higher doping levels are needed for these diester dopants to maximize conductivity in P3HT, as shown by increased polaron density in optical spectra. Viewed broadly, these results provide a pathway for future dopant molecule design with controlled solubility/miscibility as a synthetic design parameter. Future studies will include a variety of ester -R groups that could tailor the placement of molecular dopants with respect to particular conjugated molecules/polymers.

ASSOCIATED CONTENT

Supporting Information

The Supporting Information is available free of charge on the ACS Publications website at DOI: 10.1021/acs.chemmater.5b02340.

Detailed synthetic procedures and NMR, mass, UV-vis, and photoluminescence spectra (PDF)

AUTHOR INFORMATION

Corresponding Authors

*E-mail: mjmascal@ucdavis.edu.

*E-mail: amoule@ucdavis.edu.

Author Contributions

[†]J.L. and G.Z. contributed equally to this work

Notes

The authors declare no competing financial interest.

ACKNOWLEDGMENTS

This research project was supported by the U.S. Department of Energy, Office of Basic Energy Sciences, Division of Materials Sciences and Engineering, under Award DE-SC0010419.

REFERENCES

- (1) Forrest, S. R. The path to ubiquitous and low-cost organic electronic appliances on plastic. *Nature* **2004**, *428*, 911–918.
- (2) Gunes, S.; Neugebauer, H.; Sariciftci, N. S. Conjugated Polymer-Based Organic Solar Cells. *Chem. Rev.* **2007**, *107*, 1324–1338.
- (3) Cheng, Y.-J.; Yang, S.-H.; Hsu, C.-S. Synthesis of Conjugated Polymers for Organic Solar Cell Applications. *Chem. Rev.* **2009**, *109*, 5868–5923.
- (4) Lussem, B.; Riede, M.; Leo, K. Doping of organic semiconductors. *Phys. Status Solidi A* **2013**, *210*, 9–43.
- (5) Zhou, X.; Blochwitz, J.; Pfeiffer, M.; Nollau, A.; Fritz, T.; Leo, K. Enhanced Hole Injection into Amorphous Hole-Transport Layers of Organic Light-Emitting Diodes Using Controlled p-Type Doping. *Adv. Funct. Mater.* **2001**, *11*, 310–314.
- (6) Reineke, S.; Thomschke, M.; Lussem, B.; Leo, K. White organic light-emitting diodes: Status and perspective. *Rev. Mod. Phys.* **2013**, *85*, 1245–1293.
- (7) Taima, T.; Sakai, J.; Yamanari, T.; Saito, K. Doping effects for organic photovoltaic cells based on small-molecular-weight semiconductors. *Sol. Energy Mater. Sol. Cells* **2009**, *93*, 742–745.

- (8) Hains, A. W.; Liang, Z.; Woodhouse, M. A.; Gregg, B. A. Molecular Semiconductors in Organic Photovoltaic Cells. *Chem. Rev.* **2010**, *110*, 6689–6735.
- (9) Braga, D.; Horowitz, G. High-Performance Organic Field-Effect Transistors. *Adv. Mater.* **2009**, *21*, 1473–1486.
- (10) Lu, G.; Blakesley, J.; Himmelberger, S.; Pingel, P.; Frisch, J.; Lieberwirth, I.; Salzman, I.; Oehzelt, M.; di Pietro, R.; Salleo, A.; Koch, N.; Neher, D. Moderate doping leads to high performance of semiconductor/insulator polymer blend transistors. *Nat. Commun.* **2013**, *4*, 1588.
- (11) Heeger, A. J.; Sariciftci, N. S.; Nardas, E. B. *Semiconducting and Metallic Polymers*; Oxford University Press: Oxford, U.K., 2010.
- (12) Jonsson, S.; Birgersson, J.; Crispin, X.; Greczynski, G.; Osikowicz, W.; van der Gon, A. D.; Salaneck, W.; Fahlman, M. The effects of solvents on the morphology and sheet resistance in poly(3,4-ethylenedioxythiophene)-polystyrenesulfonic acid (PEDOT-PSS) films. *Synth. Met.* **2003**, *139*, 1–10.
- (13) Elschner, A.; Kirchmeyer, S. *PEDOT-Type Materials in Organic Solar Cells*; Wiley-vch: Weinheim, Germany, 2008.
- (14) Walzer, K.; Maennig, B.; Pfeiffer, M.; Leo, K. Highly Efficient Organic Devices Based on Electrically Doped Transport Layers. *Chem. Rev.* **2007**, *107*, 1233–1271.
- (15) Brédas, J.; Wudl, F.; Heeger, A. Polarons and bipolarons in doped polythiophene: A theoretical investigation. *Solid State Commun.* **1987**, *63*, 577–580.
- (16) Colaneri, N.; Nowak, M.; Spiegel, D.; Hotta, S.; Heeger, A. J. Bipolarons in poly(3-methylthiophene): Spectroscopic, magnetic, and electrochemical measurements. *Phys. Rev. B: Condens. Matter Mater. Phys.* **1987**, *36*, 7964–7968.
- (17) Aziz, E.; Vollmer, A.; Eisebitt, S.; Eberhardt, W.; Pingel, P.; Neher, D.; Koch, N. Localized Charge Transfer in a Molecularly Doped Conducting Polymer. *Adv. Mater.* **2007**, *19*, 3257–3260.
- (18) Panda, P.; Veldman, D.; Sweelssen, J.; Bastiaansen, J. J. A. M.; Langeveld-Voss, B. M. W.; Meskers, S. C. J. Charge Transfer Absorption for -Conjugated Polymers and Oligomers Mixed with Electron Acceptors. *J. Phys. Chem. B* **2007**, *111*, 5076–5081.
- (19) Zhu, L.; Kim, E.-G.; Yi, Y.; Brédas, J.-L. Charge Transfer in Molecular Complexes with 2,3,5,6-Tetrafluoro-7,7,8,8-tetracyanoquinodimethane (F4-TCNQ): A Density Functional Theory Study. *Chem. Mater.* **2011**, *23*, 5149–5159.
- (20) Gao, J.; Roehling, J. D.; Li, Y.; Guo, H.; Moule, A. J.; Grey, J. K. The effect of 2,3,5,6-tetrafluoro-7,7,8,8-tetracyanoquinodimethane charge transfer dopants on the conformation and aggregation of poly(3-hexylthiophene). *J. Mater. Chem. C* **2013**, *1*, S638–S646.
- (21) Kearns, D. R.; Tollin, G.; Calvin, M. Electrical properties of organic solids. II. Effects of added electron acceptor on metal-free phthalocyanine. *J. Chem. Phys.* **1960**, *32*, 1020–1025.
- (22) Chen, E. C. M.; Wentworth, W. E. A comparison of experimental determinations of electron affinities of pi charge transfer complex acceptors. *J. Chem. Phys.* **1975**, *63*, 3183–3191.
- (23) Cooper, C. D.; Frey, W. F.; Compton, R. N. Negative ion properties of fluoranil, chloranil, and bromanil: Electron affinities. *J. Chem. Phys.* **1978**, *69*, 2367–2374.
- (24) Ferraris, J.; Cowan, D. O.; Walatka, V.; Perlstein, J. H. Electron transfer in a new highly conducting donor-acceptor complex. *J. Am. Chem. Soc.* **1973**, *95*, 948–949.
- (25) Compton, R. N.; Cooper, C. D. Negative ion properties of tetracyanoquinodimethane: Electron affinity and compound states. *J. Chem. Phys.* **1977**, *66*, 4325–4329.
- (26) Maitrot, M.; Guillaud, G.; Boudjema, B.; André, J. J.; Simon, J. Molecular material-based junctions: Formation of a Schottky contact with metallophthalocyanine thin films doped by the cosublimation method. *J. Appl. Phys.* **1986**, *60*, 2396–2400.
- (27) Krikor, H.; Nagels, P. Structural characterization and electrical conductivity of poly(phenylethynyl) copper doped with iodine and 2,3-dichloro-5,6-dicyano-p-benzoquinone. *Synth. Met.* **1989**, *29*, 109–114.
- (28) Tolbert, L.; Edmond, C.; Kowalik, J. Charge-transfer doping of poly(3-alkyl-2,2'-bithiophene). *Synth. Met.* **1999**, *101*, 500–501.
- (29) Pingel, P.; Schwarzl, R.; Neher, D. Effect of molecular p-doping on hole density and mobility in poly(3-hexylthiophene). *Appl. Phys. Lett.* **2012**, *100*, 143303.
- (30) Wang, C.; Duong, D. T.; Vandewal, K.; Rivnay, J.; Salleo, A. Optical measurement of doping efficiency in poly(3-hexylthiophene) solutions and thin films. *Phys. Rev. B: Condens. Matter Mater. Phys.* **2015**, *91*, 085205.
- (31) Koech, P. K.; Padmaperuma, A. B.; Wang, L.; Swensen, J. S.; Polikarpov, E.; Darsell, J. T.; Rainbolt, J. E.; Gaspar, D. J. Synthesis and Application of 1,3,4,5,7,8-Hexafluorotetracyanonaphthoquinodimethane (F6-TNAP): A Conductivity Dopant for Organic Light-Emitting Devices. *Chem. Mater.* **2010**, *22*, 3926–3932.
- (32) Tietze, M. L.; Burtone, L.; Riede, M.; Lüssem, B.; Leo, K. Fermi level shift and doping efficiency in p-doped small molecule organic semiconductors: A photoelectron spectroscopy and theoretical study. *Phys. Rev. B: Condens. Matter Mater. Phys.* **2012**, *86*, 035320.
- (33) Gao, Z. Q.; Mi, B. X.; Xu, G. Z.; Wan, Y. Q.; Gong, M. L.; Cheah, K. W.; Chen, C. H. An organic p-type dopant with high thermal stability for an organic semiconductor. *Chem. Commun.* **2008**, 117–119.
- (34) Schulze, K.; Urich, C.; Schüppel, R.; Leo, K.; Pfeiffer, M.; Brier, E.; Reinold, E.; Bäuerle, P. Efficient Vacuum-Deposited Organic Solar Cells Based on a New Low-Bandgap Oligothiophene and Fullerene C60. *Adv. Mater.* **2006**, *18*, 2872–2875.
- (35) Meerheim, R.; Olthof, S.; Hermenau, M.; Scholz, S.; Petrich, A.; Tessler, N.; Solomeshch, O.; Lüssem, B.; Riede, M.; Leo, K. Investigation of C60F36 as low-volatility p-dopant in organic optoelectronic devices. *J. Appl. Phys.* **2011**, *109*, 103102.
- (36) Solomeshch, O.; Yu, Y. J.; Goryunkov, A. A.; Sidorov, L. N.; Tuktarov, R. F.; Choi, D. H.; Jin, J.-I.; Tessler, N. Ground-State Interaction and Electrical Doping of Fluorinated C60 in Conjugated Polymers. *Adv. Mater.* **2009**, *21*, 4456–4460.
- (37) Falkenberg, C.; Olthof, S.; Rieger, R.; Baumgarten, M.; Muellen, K.; Leo, K.; Riede, M. The role of energy level matching in organic solar cells—Hexaazatriphenylene hexacarbonitrile as transparent electron transport material. *Sol. Energy Mater. Sol. Cells* **2011**, *95*, 927–932.
- (38) Diouf, B. B.; Jeon, W. S.; Park, J. S.; Choi, J. W.; Son, Y. H.; Lim, D. C.; Doh, Y. J.; Kwon, J. H. High hole mobility through charge recombination interface in organic light-emitting diodes. *Synth. Met.* **2011**, *161*, 2087–2091.
- (39) Lin, H.; Lin, W.; Chang, J.; Wu, C. Solution-processed hexaazatriphenylene hexacarbonitrile as a universal hole-injection layer for organic light-emitting diodes. *Org. Electron.* **2013**, *14*, 1204–1210.
- (40) Veyssel, A. V.; De Sio, A.; Riedel, D.; Deschler, F.; Como, E. D.; Parisi, J.; von Hauff, E. Molecular doping of low-bandgap-polymer-fullerene solar cells: Effects on transport and solar cells. *Org. Electron.* **2012**, *13*, 290–296.
- (41) Rainbolt, J. E.; Koech, P. K.; Polikarpov, E.; Swensen, J. S.; Cosimbescu, L.; von Ruden, A.; Wang, L.; Sapochak, L. S.; Padmaperuma, A. B.; Gaspar, D. J. Synthesis and characterization of p-type conductivity dopant 2-(3-(adamantan-1-yl)propyl)-3,5,6-trifluoro-7,7,8,8-tetracyanoquinodimethane. *J. Mater. Chem. C* **2013**, *1*, 1876–1884.
- (42) Arias, A. C.; MacKenzie, J. D.; McCulloch, I.; Rivnay, J.; Salleo, A. Materials and Applications for Large Area Electronics: Solution-Based Approaches. *Chem. Rev.* **2010**, *110*, 3–24.
- (43) Pinal, R. Effect of molecular symmetry on melting temperature and solubility. *Org. Biomol. Chem.* **2004**, *2*, 2692–2699.
- (44) Andersson, M. R.; Berggren, M.; Inganäs, O.; Gustafsson, G.; Gustafsson-Carlberg, J. C.; Selse, D.; Hjertberg, T.; Wennerström, O. Electroluminescence from Substituted Poly(thiophenes): From Blue to Near-Infrared. *Macromolecules* **1995**, *28*, 7525–7529.
- (45) D'Andrade, B. W.; Datta, S.; Forrest, S. R.; Djurovich, P.; Polikarpov, E.; Thompson, M. E. Relationship between the ionization and oxidation potentials of molecular organic semiconductors. *Org. Electron.* **2005**, *6*, 11–20.
- (46) Gao, W.; Kahn, A. Controlled p-doping of zinc phthalocyanine by coevaporation with tetrafluorotetracyanoquinodimethane: A direct

- 752 and inverse photoemission study. *Appl. Phys. Lett.* **2001**, *79*, 4040–
753 4042.
- 754 (47) Österbacka, R.; An, C. P.; Jiang, X. M.; Vardeny, Z. V. Two-
755 Dimensional Electronic Excitations in Self-Assembled Conjugated
756 Polymer Nanocrystals. *Science* **2000**, *287*, 839–842.
- 757 (48) Hwang, I.-W.; Moses, D.; Heeger, A. J. Photoinduced Carrier
758 Generation in P3HT/PCBM Bulk Heterojunction Materials. *J. Phys.*
759 *Chem. C* **2008**, *112*, 4350–4354.
- 760 (49) Lloyd, M. T.; Prasankumar, R. P.; Sinclair, M. B.; Mayer, A. C.;
761 Olson, D. C.; Hsu, J. W. P. Impact of interfacial polymer morphology
762 on photoexcitation dynamics and device performance in P3HT/ZnO
763 heterojunctions. *J. Mater. Chem.* **2009**, *19*, 4609–4614.
- 764 (50) Bouman, M. M.; Havinga, E. E.; Janssen, R. A. J.; Meijer, E. W.
765 Chiroptical Properties of Regioregular Chiral Polythiophenes. *Mol.*
766 *Cryst. Liq. Cryst. Sci. Technol., Sect. A* **1994**, *256*, 439–448.
- 767 (51) Moulé, A. J.; Meerholz, K. Controlling Morphology in Polymer-
768 Fullerene Mixtures. *Adv. Mater.* **2008**, *20*, 240–245.
- 769 (52) Duong, D. T.; Wang, C.; Antono, E.; Toney, M. F.; Salleo, A.
770 The chemical and structural origin of efficient p-type doping in P3HT.
771 *Org. Electron.* **2013**, *14*, 1330–1336.
- 772 (53) Yim, K. H.; Whiting, G. L.; Murphy, C. E.; Halls, J. J. M.;
773 Burroughes, J. H.; Friend, R. H.; Kim, J.-S. Controlling Electrical
774 Properties of Conjugated Polymers via a Solution-Based p-Type
775 Doping. *Adv. Mater.* **2008**, *20*, 3319–3324.
- 776 (54) Pingel, P.; Neher, D. Comprehensive picture of p-type doping of
777 P3HT with the molecular acceptor F4TCNQ. *Phys. Rev. B: Condens.*
778 *Matter Mater. Phys.* **2013**, *87*, 115209.
- 779 (55) Noriega, R.; Rivnay, J.; Vandewal, K.; Koch, F. P. V.; Stingelin,
780 N.; Smith, P.; Toney, M. F.; Salleo, A. A general relationship between
781 disorder, aggregation and charge transport in conjugated polymers.
782 *Nat. Mater.* **2013**, *12*, 1037–1043.
- 783 (56) Koch, F. P. V.; et al. The impact of molecular weight on
784 microstructure and charge transport in semicrystalline polymer
785 semiconductors-poly(3-hexylthiophene), a model study. *Prog. Polym.*
786 *Sci.* **2013**, *38*, 1978–1989. Topical issue on Conductive Polymers.
- 787 (57) Clark, J.; Silva, C.; Friend, R. H.; Spano, F. C. Role of
788 Intermolecular Coupling in the Photophysics of Disordered Organic
789 Semiconductors: Aggregate Emission in Regioregular Polythiophene.
790 *Phys. Rev. Lett.* **2007**, *98*, 206406.
- 791 (58) Chang, L.; Lademann, H. W. A.; Bonekamp, J.-B.; Meerholz, K.;
792 Moulé, A. J. Effect of Trace Solvent on the Morphology of
793 P3HT:PCBM Bulk Heterojunction Solar Cells. *Adv. Funct. Mater.*
794 **2011**, *21*, 1779–1787.
- 795 (59) Roehling, J. D.; Arslan, I.; Moule, A. J. Controlling
796 microstructure in poly(3-hexylthiophene) nanofibers. *J. Mater. Chem.*
797 **2012**, *22*, 2498–2506.
- 798 (60) Jacobs, I. E.; Li, J.; Burg, S. L.; Bilsky, D. J.; Rotondo, B. T.;
799 Augustine, M. P.; Stroeve, P.; Moulé, A. J. Reversible Optical Control
800 of Conjugated Polymer Solubility with Sub-micrometer Resolution.
801 *ACS Nano* **2015**, *9*, 1905–1912.
- 802 (61) Tsoi, W. C.; Spencer, S. J.; Yang, L.; Ballantyne, A. M.;
803 Nicholson, P. G.; Turnbull, A.; Shard, A. G.; Murphy, C. E.; Bradley,
804 D. D. C.; Nelson, J.; Kim, J.-S. Effect of Crystallization on the
805 Electronic Energy Levels and Thin Film Morphology of P3HT:PCBM
806 Blends. *Macromolecules* **2011**, *44*, 2944–2952.
- 807 (62) Ferguson, A. J.; Kopidakis, N.; Shaheen, S. E.; Rumbles, G.
808 Quenching of Excitons by Holes in Poly(3-hexylthiophene) Films. *J.*
809 *Phys. Chem. C* **2008**, *112*, 9865–9871.
- 810 (63) Mauger, S. A.; Li, J.; Ozmen, O. T.; Yang, A. Y.; Friedrich, S.;
811 Rail, M. D.; Berben, L. A.; Moule, A. J. High work-function hole
812 transport layers by self-assembly using a fluorinated additive. *J. Mater.*
813 *Chem. C* **2014**, *2*, 115–123.
- 814 (64) Nardes, A. M.; Kemerink, M.; Janssen, R. A. J.; Bastiaansen, J. A.
815 M.; Kiggen, N. M. M.; Langeveld, B. M. W.; van Breemen, A.; de Kok,
816 M. M. Microscopic understanding of the anisotropic conductivity of
817 PEDOT:PSS thin films. *Adv. Mater.* **2007**, *19*, 1196–1200.